Differences between Nonprecipitating Tropical and Trade Wind Marine Shallow Cumuli

VIRENDRA P. GHATE

Environmental Science Division, Argonne National Laboratory, Argonne, Illinois

MARK A. MILLER

Department of Environmental Sciences, Rutgers, The State University of New Jersey, New Brunswick, New Jersey

PING ZHU

Department of Earth Sciences, Florida International University, University Park, Florida

(Manuscript received 24 March 2015, in final form 19 October 2015)

ABSTRACT

Marine nonprecipitating cumulus topped boundary layers (CTBLs) observed in a tropical and in a trade wind region are contrasted based on their cloud macrophysical, dynamical, and radiative structures. Data from the Atmospheric Radiation Measurement (ARM) observational site previously operating at Manus Island, Papua New Guinea, and data collected during the deployment of ARM Mobile Facility at the island of Graciosa, in the Azores, were used in this study. The tropical marine CTBLs were deeper, had higher surface fluxes and boundary layer radiative cooling, but lower wind speeds compared to their trade wind counterparts. The radiative velocity scale was 50%–70% of the surface convective velocity scale at both locations, highlighting the prominent role played by radiation in maintaining turbulence in marine CTBLs. Despite greater thicknesses, the chord lengths of tropical cumuli were on average lower than those of trade wind cumuli, and as a result of lower cloud cover, the hourly averaged (cloudy and clear) liquid water paths of tropical cumuli were lower than the trade wind cumuli. At both locations ~70% of the cloudy profiles were updrafts, while the average amount of updrafts near cloud base stronger than 1 m s^{-1} was ~22% in tropical cumuli and ~12% in the trade wind cumuli. The mean in-cloud radar reflectivity within updrafts and mean updraft velocity was higher in tropical cumuli than the trade wind cumuli. Despite stronger vertical velocities and a higher number of strong updrafts, due to lower cloud fraction, the updraft mass flux was lower in the tropical cumuli compared to the trade wind cumuli. The observations suggest that the tropical and trade wind marine cumulus clouds differ significantly in their macrophysical and dynamical structures.

1. Introduction

Boundary layer (BL) shallow cumulus clouds play a vital role in Earth's atmospheric system. These clouds are ubiquitous and are routinely observed over the land and over the oceans from the tropics to the poles (Eastman and Warren 2013; Eastman and Warren 2014). These clouds are closely linked to turbulence within the marine boundary layer that is primarily driven by the surface turbulent fluxes, radiative cooling, and wind shear. The shallow cumuli observed over the tropical and subtropical oceans cover vast areas, and have a significant impact on Earth's radiation budget and upon the energy and water cycles (Neggers et al. 2007; Long et al. 2013). Hence, it is necessary to accurately represent these clouds in global climate model (GCM) simulations used to predict future climate and energy needs. Because these clouds occur at spatial and temporal scales much smaller than the GCM grid resolution and iteration time step, their effects and those of the relevant processes underlying them need to be parameterized in GCMs (Arakawa 2004).

Marine boundary layer cumulus clouds have been the focus of several past field campaigns including the Atlantic Trade Wind Experiment (ATEX; Augstein et al.

Corresponding author address: Virendra P. Ghate, Environmental Science Division, Argonne National Laboratory, 9700 S. Cass Ave., Argonne, IL 60439.
E-mail: vghate@anl.gov

DOI: 10.1175/MWR-D-15-0110.1

1973, 1974), the Barbados Oceanographic and Meteorological Experiment (BOMEX; Davidson 1968), Rain in Cumulus over Ocean (RICO; Rauber et al. 2007), and others. Data from these field campaigns and data collected at other locations have been extensively used in observational and modeling studies aimed at improving our understanding of these clouds (e.g., Li et al. 2014; Nuijens and Stevens 2012). Some of the previous studies have focused on evaluating cumulus parameterizations (e.g., Golaz et al. 2005; Lappen et al. 2010; Larson et al. 2012) and model intercomparison studies (e.g., Siebesma et al. 2003; Stevens et al. 2001; vanZanten et al. 2011). Despite these efforts, shallow cumulus clouds are poorly represented in the GCM used in the fifth phase of the Coupled Model Intercomparison Project (CMIP5; Nam et al. 2012; Klein et al. 2013).

Several parameterizations have been proposed to represent cumulus clouds in GCMs (e.g., Albrecht et al. 1979; Bretherton and Park 2008; Berg et al. 2013; Lappen et al. 2010; Golaz et al. 2002; Bretherton et al. 2004). The more sophisticated of these parameterizations are tied to the boundary layer schemes as these clouds heavily modulate and are also modulated by the turbulence within the boundary layer. The cumulus parameterizations based on the higher-order turbulence closure, plume decomposition, and PDF-based approaches use some measure of vertical air motion to diagnose the cloudiness within the GCM grid cell. To address the modeling need to understand the relationship between cloudiness and vertical air motion, in recent years several observational studies have characterized the vertical air motion within these clouds using data from in situ and remote sensing instruments (e.g., Kollias and Albrecht 2010; Ghate et al. 2011; Chandra et al. 2013; Rémillard et al. 2012; Wang and Geerts 2013). Most of the past studies have focused on one (or two) cloud type at a specific location, with fewer studies focusing on marine cumulus clouds (e.g., Nuijens et al. 2014; Ghate et al. 2011; Kollias and Albrecht 2010).

In GCM cumulus parameterizations the subgrid-scale cumulus cloudiness and associated processes are parameterized based on the resolved large-scale properties that are expected to differ between the tropics and the trade wind region. The cumulus lifetime and life cycle are not only affected by the large-scale forcing such as surface fluxes, subsidence, and winds, but also by internal cloud processes such as cloud-top radiative cooling, microphysics, and precipitation. In this study, we have characterized the external large-scale forcing variables from the reanalysis models, and have attempted to characterize the internal (subgrid) scale variables like radiation and cloud microphysics.

We have used data collected at the Atmospheric Radiation Measurement (ARM) observing facility previously operating at Manus Island in the tropical western Pacific and data collected during the deployment of the first ARM Mobile Facility (AMF-1) at the island of Graciosa in the eastern North Atlantic. The focus of this paper is on marine boundary layers with tops of cumulus clouds lower than 1 km that are devoid of any precipitation. The data, radiative transfer model, and the methodology are described in the next section, which is followed by a description of the general conditions together with the boundary layer thermodynamic and radiative structure at the two locations. The in-cloud dynamical structures observed at the two locations are compared and reported upon in section 4, which is followed by a summary and discussion section.

2. Data, radiative transfer model, and methodology

Below is a description of the case selection criteria and the instrumentation at each location along with the operational setting of the radiative transfer model and the methodology. We only describe the instrumentation at the two facilities that are used in this study, but all instrumentation at the two facilities is described in detail in Mather and Voyles (2013) and Long et al. (2013). Tables reporting the dates and times of the selected cases from the two locations along with the mean values of various parameters during those cases can be obtained from the first author.

a. Instrumentation and case selection criteria

The AMF-1 was deployed at the island of Graciosa in the eastern North Atlantic (39.08°N, 28.01°W, 15.24-m elevation) for a 19-month period from June 2009 to December 2010 (Wood et al. 2015). The facility was located at the northern edge of the island with an aim of sampling trade wind clouds unperturbed by the island heating or topography during northerly wind conditions. A vertically pointing Doppler cloud radar operating at 95-GHz frequency and termed the W-band ARM Cloud Radar (WACR) was part of the AMF-1 instrumentation along with a ceilometer, microwave radiometer, and surface meteorological station. The WACR recorded the full Doppler spectrum at a 2-s temporal and 42-m range resolution from which the first three moments of the Doppler spectrum (reflectivity, mean Doppler velocity, and Doppler spectrum width) were calculated. The ceilometer operated at 905-nm wavelength and recorded the first three cloud-base heights at 15-s temporal and 30-m range resolution. Filtered radar reflectivity and cloud boundaries were retrieved by combining the WACR data together with that of the ceilometer using

TABLE 1. The location, number of cumulus cases, number of hours, number of hours during which clouds were detected by the ceilometer, number of hours available for dynamical retrieval, total number of radiosonde launches, daytime hours, nighttime hours, and hours during four different seasons are reported for the Azores and Manus.

	Azores	Manus
Location	39.08°N, 28.01°W	2.05°S, 147.41°E
No. of cases	14	19
No. of hours	200	306
Detected by ceilometer (h)	179 (89%)	260 (85%)
Available for dynamical retrievals (h)	166 (83%)	197 (64%)
No. of soundings	43	34
Daytime hours ($SWD_{sfc} > 100\,W\,m^{-2}$)	93 (46%)	98 (32%)
Nighttime hours ($SWD_{sfc} < 0\,W\,m^{-2}$)	71 (35%)	158 (51%)
No. of MAM cases (h)	1 (13)	9 (101)
No. of JJA cases (h)	4 (53)	3 (25)
No. of SON cases (h)	7 (82)	4 (33)
No. of DJF cases (h)	2 (18)	3 (38)

the technique presented by Kollias et al. (2009). The microwave radiometer (MWR) recorded the sky brightness temperatures at 23 and 32 GHz, from which the column-integrated water vapor (IWV) and liquid water path (LWP) were retrieved. A radiation tower that is part of the AMF-1 recorded the surface downwelling shortwave and longwave radiation at 1-min temporal resolution. Balloon-borne radiosondes were launched at the AMF-1 every 6 h (0000, 0600, 1200, and 1800 UTC) and recorded the temperature, pressure, humidity, and winds in the troposphere. Similar to Ghate et al. (2011), in this study we identified cases of marine cumulus clouds that adhered to the following conditions: 1) boundary layer cumuli are observed for at least three consecutive hours, 2) winds in the boundary layer were from the north, 3) no heavy precipitation was recorded by the cloud radar (reflectivity >0 dBZ), 4) the hourly averaged cloud-top height was lower than 3 km, 5) the ceilometer-recorded cloud cover was less than 50%, and 6) the cloud-top temperature was higher than 0°C. These criteria yielded 14 cases lasting for 200 h (Table 1). As the facility was within 50 m of the northern edge of the island, we anticipate minimal influence from the island on the observed clouds.

The ARM observing facility previously present at the Manus Island was located along the eastern edge of the island (2.05°S, 147.41°W, 4-m elevation) and was active from 1997 until 2014 (Long et al. 2013). A vertically pointing Doppler cloud radar operating at 35-GHz frequency was present at the ARM facility in Manus and was referred to as the Millimeter Cloud Radar (MMCR). The MMCR was functioning in several different operational modes designed to observe all cloud types (Kollias et al. 2007). Data from all of the MMCR operational modes were combined to yield filtered radar Doppler spectrum moments and cloud boundaries at 10-s and 45-m resolution (Clothiaux et al. 2000). Similar to AMF-1, a ceilometer, microwave radiometer, surface meteorological station, and radiation tower were included in the instrumentation at Manus. Balloon-borne radiosondes were also launched at the site, albeit only twice a day, at 0000 and 1200 UTC. In this study, we searched through the data collected at Manus between 2005 and 2008 to identify cases of oceanic shallow cumulus clouds. By using a similar set of six criteria as was done for the Azores to identify shallow cumulus clouds (except with the easterly wind direction in place of the northerly), 19 cases spanning over 306 h were identified. As there are few small islands east of Manus Island, some land influence on the observed clouds cannot be dismissed. However, the shallow nature of the observed cumuli (cloud tops lower than 1500 m) suggests the clouds to be of oceanic origin.

Because of the transient nature of the shallow cumulus clouds and the associated low values of cloud coverage, out of the total 200 h of data at the Azores, within time bins of 1 h, clouds were detected by the ceilometer during 179 h (89%). While out of the 306 h of data at Manus, within time bins of 1 h, clouds were detected by the ceilometer during 260 h (85%). From the Azores data, 93 h (46.5%) were identified as daytime using the criteria of the downwelling shortwave radiation at the surface being greater than $100\,W\,m^{-2}$, while 71 h (35.5%) were identified as nighttime using the criteria of no downwelling shortwave radiation at the surface. Similarly, 98 h (32%) were identified as daytime from the Manus dataset and 158 h (51%) were identified as nighttime. The day–night classification of the data suggest that the marine cumuli were observed at both locations during the daytime and nighttime, contrary to shallow cumuli over land that predominantly occur during the late afternoon (Zhang and Klein 2013).

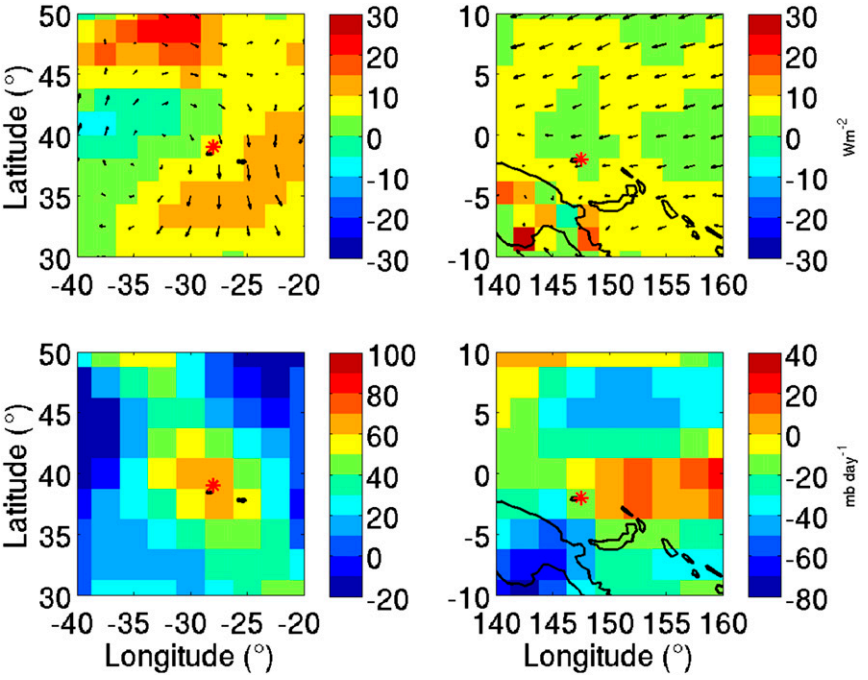

FIG. 1. Latitude–longitude maps of (top) surface SHF and (bottom) 700-mb subsidence rate for (left) the Azores and (right) Manus as reported by the NCEP–NCAR reanalysis. The shown values are averages calculated from the selected cases. The locations of the sites are shown in the panels by red asterisks, and the average winds are shown in the top panels. The ARM facility was located along the northern edge of the island in the Azores, and along the eastern edge of the island in Manus.

The National Centers for Environmental Prediction–National Center for Atmospheric Research (NCEP–NCAR) reanalysis (Kalnay et al. 1996) reported that averaged surface sensible heat fluxes were largely uniform at the two locations (Fig. 1) for the selected cases, with the averaged large-scale wind patterns consistent with the chosen wind directions. The surface sensible heat fluxes at both locations were low (around $\pm 10\,\mathrm{W\,m^{-2}}$). The average large-scale vertical velocity at 700 mb (1 mb = 1 hPa) was always positive (downward motion) over the Azores region, with values of $\sim 70\,\mathrm{mb\,day^{-1}}$ near the site. Over the region close to the ARM Manus site, because of the tropical location, the subsidence rate was low (around $\pm 20\,\mathrm{mb\,day^{-1}}$) with positive values due east of the site and negative values in all other directions. As shallow cumulus clouds often form under suppressed conditions, this further reinforces the choice of the wind direction in case identification.

The averaged cloud fraction as a function of height from the selected cases is shown in Fig. 2. The shown values of cloud fraction have been calculated from all the 200 h of data available at the Azores, and 306 h of data available at Manus, and before applying the threshold of $-15\,\mathrm{dB}Z$ to remove precipitation (discussed later).

Although the mean cloud covers calculated from ceilometer observations at the two locations are 14.33% (Manus) and 19.58% (the Azores), the highest cloud fraction values at a given height are less than 5% at each location. The peak value in cloud fraction at the Azores is ~4.3%, while that at Manus is ~2.1%. Because of higher cumulus-cloud-top heights over Manus as compared to the Azores (Table 2), the peak in cloud fraction associated with cumulus clouds is at a higher altitude over Manus than at the Azores. Both locations show a secondary peak in cloud fraction associated with cirrus clouds that peak around 11 km to ~0.5% over the Azores and around 13 km over Manus to 1.9%. The thickness of the cirrus layer is ~7 km at both locations with the cirrus clouds occurring from 6 to 13 km at the Azores and from 8 to 15 km at Manus. The cloud fraction of cirrus clouds and that of the cumulus clouds are similar over Manus, while at the Azores the cumulus cloud fraction is almost 8 times that of the cirrus cloud fraction. A few transient stratocumulus clouds were observed in the Azores (e.g., on 15 September and 10 October 2009) above the cumulus-topped boundary layer that were not physically connected to the cumulus cloud field.

b. *Radiative transfer model*

In this study, we have used a one-dimensional radiative transfer model known as the Rapid Radiative Transfer Model (RRTM) to calculate profiles of

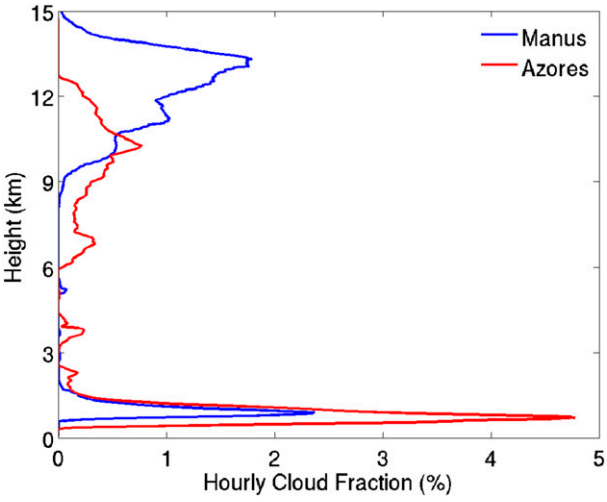

FIG. 2. Averaged vertical profile of hourly cloud fraction during cumulus clouds conditions at Manus (blue) and the Azores (red). The shown values are calculated from the 200 h of data available at the Azores and from the 306 h of data available at Manus, and before applying the threshold of −15 dBZ to remove precipitation.

broadband radiative fluxes and radiative heating rates at the two locations for the selected cases (Iacono et al. 2000; Morcrette et al. 2001). RRTM uses a correlated-K approach and has total of 29 bands within the shortwave and longwave spectra. Because of the transient nature of the shallow cumulus clouds, these clouds lingered over the cloud radar for only a few minutes. This necessitated the RRTM simulations to be made at high temporal and spatial resolution. To be consistent with the cloud radar observations, RRTM runs were made for every cloud-radar-reported profile of filtered reflectivity. Hence, the RRTM simulations were made at 10-s and 45-m resolution for cases from Manus and at 5-s and 42-m resolution for cases from the Azores. It is beyond the scope of this study to assess the impacts of RRTM temporal resolution on the calculated radiative fluxes, but we expect them to be minimal.

The inputs to the RRTM were consistent with those found by Mather et al. (2007) and Ghate et al. (2015), in which the vertical profiles of temperature and water vapor mixing ratio as reported by the mergesonde value-added product (Troyan 2012) were used. The cloud liquid water content (LWC) profile was estimated using the reflectivity–LWC relationship proposed by Matrosov et al. (2004) and the cloud ice water content (IWC) was retrieved using the reflectivity–IWC relationship proposed by Liu and Illingworth (2000). The cloud droplet effective radius for liquid clouds was estimated by assuming a lognormal drop size distribution with a width of 0.35 and droplet number concentration of 74 cm^{-3}, as reported by Miles et al. (2000), and the effective radius for ice cloud was retrieved using the temperature-dependent relationship proposed by Ivanova et al. (2001). None of the boundary layer cumuli contained ice and were warm (>0°C), while it was necessary to use the reflectivity–IWC relationship to properly simulate the radiative effects of cirrus clouds. The ARM cloud radars are calibrated within ±3 dB; hence, a 6-dB change in the radar reflectivity will yield a 0.16 g m^{-3} change in retrieved LWC, as well as a 2.8-μm change in effective radius, impacting the radiative transfer calculations.

The latest greenhouse gas concentrations as reported by the Carbon Dioxide Analysis Center were used, with that of CO_2 being 400 ppm. We are aware that the method used to estimate microphysical quantities has a significant impact on the calculated radiative fluxes, especially for ice clouds (Comstock et al. 2013). But given the shallowness of these clouds and their minimal coverage, we believe that this sensitivity is likely to play a minor role in the total radiation budget.

c. *Methodology*

Hourly values of one-dimensional cloud fraction (termed cloud cover) of boundary layer clouds were determined by using the ceilometer-reported first cloud-base heights below 3 km at each site. Hourly values of cloud-top height, cloud-base height, cloud thickness, IWV, and LWP were also calculated. The output from the RRTM simulations was used to calculate the hourly averaged values of radiative fluxes, heating rates, and the radiative flux divergence across the cloud layer. The number of individual cloud elements observed in each case was also identified by locating temporal gaps in the radar reflectivity data below 3 km that are greater than 20 s. Additionally, if the temporal gap in the radar reflectivity was less than 10 s, the two elements were considered to belong to the same cloud mass. The identification of individual cloud elements was necessary to calculate the cloud chord length, which is the product of the duration of the cloud element over the cloud radar and the horizontal wind speed at 100 m as reported by the soundings during those cases.

The surface sensible heat flux (SHF), latent heat flux (LHF), and large-scale subsidence rate at 700 mb as reported by the European Centre for Medium-Range Weather Forecasts (ECMWF) ERA-Interim model (ECMWF 1994) and NCEP–NCAR reanalysis (Kalnay et al. 1996) were used in this study. Additionally, the temperature and moisture tendency at 900 mb at the two locations were also retrieved for characterizing the boundary layer forcing. The data from the ECMWF model were available for every hour, while the data from the NCEP–NCAR reanalysis were only available every 6 h. Hence, it was not possible to

TABLE 2. The mean and standard deviation variables describing cumulus cloud properties at the two locations. The $|t|$ value for the differences between calculated mean values at the two locations assuming a two–tailed Gaussian distribution is also reported. The critical $|t|$ value for the 95% confidence interval is 1.97. Refer to the text for the details.

Parameter	Manus		Azores		$\|t\|$ value
No. of hours	197		166		
No. of cumulus elements	685		747		
	Mean	Std dev	Mean	Std dev	
Ceilometer cloud cover (%)	14.33	11.43	30.68	19.58	9.48
IWV (cm)	4.40	0.6	2.19	0.60	5.13
LWP ($g\,m^{-2}$)	34.22	21.52	42.44	30.78	2.89
Cloud base (m)	759	100	563	153	14.15
Cloud top (m)	1029	129	746	170	17.59
Cloud thickness (m)	267	95	179	33	12.15
Cloud chord length (m)	308	207	411	207	4.72
Cloud mean updraft reflectivity (dBZ)	−25.22	4.80	−29.96	4.96	9.20
Cloud mean updraft (core) velocity ($m\,s^{-1}$)	0.77	0.29	0.58	0.28	6.33
Cloud mean coherent updraft velocity ($m\,s^{-1}$)	0.80	0.32	0.61	0.33	5.54
Updraft mass flux at $\eta = 0.2$ ($g\,m^{-2}\,s^{-1}$)	13.44	21.40	21.92	31.53	3.03
Contribution of updrafts to cloud fraction at $\eta = 0.2$ (%)	69.32	27.59	71.77	18.13	0.97
Contribution of downdrafts to cloud fraction at $\eta = 0.2$ (%)	30.67	27.59	28.22	18.13	0.97
Contribution of updrafts stronger than $1\,m\,s^{-1}$ to cloud fraction at $\eta = 0.2$ (%)	22.07	23.17	12.61	13.21	4.86
Contribution of downdrafts stronger than $-1\,m\,s^{-1}$ to cloud fraction at $\eta = 0.2$ (%)	8.44	20.03	0.52	1.47	5.53
Contribution of updrafts to cloud fraction at $\eta = 0.8$ (%)	38.60	34.54	44.60	22.42	1.99
Contribution of updrafts stronger than $1\,m\,s^{-1}$ to cloud fraction at $\eta = 0.8$ (%)	12.46	27.68	15.03	14.59	1.13
Contribution of downdrafts to cloud fraction at $\eta = 0.8$ (%)	61.39	34.54	55.39	22.42	1.99
Contribution of downdrafts stronger than $-1\,m\,s^{-1}$ to cloud fraction at $\eta = 0.8$ (%)	22.03	28.57	12.78	16.44	3.85

calculate the standard deviation of variables reported by the NCEP–NCAR reanalysis and the $|t|$ values of statistical significance of differences between the two sites as a result of the low number of samples. Because of the lack of observations of surface meteorology over the ocean at both locations, the lifting condensation level (LCL) was calculated for each case (Bolton 1980) by using the average value of the temperature, relative humidity, and pressure at 100 m, as reported by the radiosondes launched during each case. Upon inspection of the individual soundings, the 100-m height was found to be sufficiently above any layer with land influence on the measurements (Ghate et al. 2015).

To quantify the impact of surface buoyancy production and boundary layer radiation on the cloud dynamics, the convective velocity scale and radiative velocity scale were calculated. The convective velocity scale due to surface-forced convection $w^*_{\rm sfc}$ was calculated using the SHF and LHF following equation per Stull (1988):

$$w^*_{\rm sfc} = \left[\frac{g \times Z_b}{\overline{\theta_v}} \times (\overline{w'\theta'_v})_{\rm sfc}\right]^{1/3}, \qquad (1)$$

where g is the acceleration due to gravity ($9.81\,m\,s^{-2}$), Z_b is the mean cloud-base height during that hour, and $\overline{\theta_v}$ is the mean virtual potential temperature at 100 m, as reported by the sounding. The mean cloud-base height was used as a scaling length in the above equation because of the inability to observe either the LCL or the mixed layer depth every hour.

The hourly values of radiative flux divergence ($\Delta F_{\rm rad}$) across the cloud layer were determined using the output from RRTM simulations. These values were further used to calculate the radiative velocity scale ($w^*_{\rm rad}$) using the equation below per Lock et al. (2000):

$$w^*_{\rm rad} = \left[\frac{g \times Z_b}{\rho \times C_p \times \overline{\theta}} \times (-\Delta F_{\rm rad})\right]^{1/3}, \qquad (2)$$

where ρ is the density of air ($1.2\,kg\,m^{-3}$), C_p is the specific heat of air at constant pressure ($1004.67\,J\,kg^{-1}\,K^{-1}$), and $\overline{\theta}$ is the mean potential temperature at 100 m, as reported by the soundings. The total convective velocity scale (w^*) was also calculated using

$$w^{*3} = w^{*3}_{\rm sfc} + w^{*3}_{\rm rad}. \qquad (3)$$

The above equation is different than that used by Lock et al. (2000), as it does not take into account the effect of wind shear and buoyancy reversal near the cloud top

because of entrainment. Because of the island location of the observing facilities, there are no observations of wind shear of the purely marine boundary layer, and to the best of our knowledge, there are no remote sensing measurement techniques available to estimate the buoyancy reversal term. Hence, we resort to using only the surface and radiative driving of the turbulence in calculating the convective velocity scale.

In the absence of precipitation-size droplets, the mean Doppler velocity as reported by a vertically pointing Doppler cloud radar can be used as a surrogate for vertical air motion (Chandra et al. 2013; Ghate et al. 2011). A threshold of $-15\,\mathrm{dB}Z$ was used to identify the presence of precipitation-size droplets and any hours that contained reflectivity values greater than $-15\,\mathrm{dB}Z$ were discarded from our analysis. A total of 166 h (83%) were identified from the Azores dataset for performing vertical velocity (dynamical) retrievals, while for the same criteria at Manus the number was 197 h (64%). *To be consistent in our analysis, we have used data from these hours only.* The exclusion of hours containing precipitation reduced the dataset by almost a fifth at the Azores, and by almost a third at Manus, suggesting the prevalence of drizzle in shallow cumuli at these locations.

Because of the broken cloud field and variable cloud depth, it was necessary to normalize the reflectivity and the retrieved vertical velocity profiles to enable statistical survey. The reflectivity and vertical velocity profiles were normalized by the maximum cloud-layer depth observed during each case. The maximum cloud-layer depth was identified by locating the minimum cloud-base height and the maximum cloud-top height for each case. The cloud-depth-normalized height was calculated using the following equation:

$$\eta(z) = \frac{Z - Z_{b\,\mathrm{min}}}{Z_{t\,\mathrm{max}} - Z_{b\,\mathrm{min}}}, \tag{4}$$

where $Z_{b\,\mathrm{min}}$ is the minimum cloud-base height and $Z_{t\,\mathrm{max}}$ is the maximum cloud-top height for each case. This method is similar to that used by Ghate et al. (2011) and preserves the identity of individual cloud elements (forced, active, or passive) in the ensemble cumulus cloud field. The cloud-layer depth-normalized reflectivity and vertical velocity values were then averaged on an hourly basis to produce hourly averaged profiles of these variables. Additionally, to be consistent with our previous work and other modeling studies (e.g., Siebesma et al. 2003), the updraft samples were identified and termed as core, and the updrafts that spanned through the entire cloud layer were termed as coherent.

The duration of the averaging period had minimal impacts on the average cloud-depth-normalized profiles of reflectivity and vertical velocity (figure not shown). When the averaging period was increased from 30 min to 3 h, the results for the vertical velocity in the middle of the cloud layer converged to similar values, while still differing near cloud boundaries. The radar reflectivity however did not show any sensitivity to changes in the averaging periods throughout the cloud-layer depth. Hence, to be consistent with the definition of the boundary layer used by Stull (1988), we chose to produce statistics on hourly time scales.

3. General characteristics

The average cloud-layer properties at the two locations are reported in Table 2, and the boundary layer properties are reported in Table 3. Also reported is the |t| value to test whether the differences between the calculated means are statistically significant assuming a two-tailed Gaussian distribution. During the 197 h of cumulus conditions over Manus, 685 individual cumulus cloud elements were identified, while during the 166 h of cumulus conditions over the Azores, 747 individual cumulus cloud elements were identified. Consistent with this, the average ceilometer-reported cloud cover was ~14% over Manus and ~30% over the Azores. The column-integrated water vapor at Manus (4.40 cm) was almost double that over the Azores (2.19 cm). This was expected because of the tropical (warmer) location of Manus and the subtropical (colder) location of the Azores. The LWP was lower ($\sim 34\,\mathrm{g\,m^{-2}}$) over Manus as compared to that over the Azores ($\sim 43\,\mathrm{g\,m^{-2}}$). The cloud bases and cloud tops were higher over Manus than over the Azores. As hourly averaged values of LWP were used in our analysis, because of the averaging of cloudy and clear-sky samples, we expect the values to be influenced by the cumulus cloud cover in addition to the cloud thickness. On average, the cumulus cloud top over the Azores (746 m) was lower than the cumulus cloud base over Manus (759 m). The cloud-layer thickness was higher over Manus (267 m) than over the Azores (179 m). These results suggest that although the clouds are on average thicker over Manus than the Azores, because of the lower cloud cover the hourly averaged LWP is lower over Manus than at the Azores. Despite the higher thickness, the cloud chord length was lower at Manus (308 m) as compared to over the Azores (411 m). We attribute this difference to higher wind speeds in the boundary layer over the Azores (Fig. 3).

The ECMWF-model-reported large-scale subsidence was weak ($4.12\,\mathrm{mb\,day^{-1}}$) over Manus during cumulus conditions as compared to the Azores ($87.7\,\mathrm{mb\,day^{-1}}$),

TABLE 3. The mean and standard deviation values of cumulus-topped boundary layer parameters at the two locations. The $|t|$ value for the differences between the calculated mean values at the two locations assuming a two-tailed Gaussian distribution is also reported. The critical $|t|$ value for the 95% confidence interval is 1.97. For some of the parameters it was not possible to calculate the $|t|$ values.

Parameter	Manus		Azores		
	Mean	Std dev	Mean	Std dev	$\|t\|$ value
NCEP ω_{700} (mb day^{-1})	−16.38	—	23.26	—	
NCEP 900 mb temp tendency (K day^{-1})	−0.85	—	−0.41	—	
NCEP 900 mb moisture tendency (g kg^{-1} day^{-1})	−2.23	—	−4.05	—	
NCEP SHF (W m^{-2})	4.98	—	3.72	—	
NCEP LHF (W m^{-2})	93.34	—	75.32	—	
ECMWF ω_{700} (mb day^{-1})	4.12	98.72	87.7	105.6	7.73
ECMWF 900 mb temp tendency (K day^{-1})	−0.28	3.34	0.11	3.71	1.04
ECMWF 900 mb moisture tendency (g kg^{-1} day^{-1})	−0.05	4.51	−1.43	4.55	2.89
ECMWF SHF (W m^{-2})	8.75	6.05	10.2	6.44	2.19
ECMWF LHF (W m^{-2})	120.69	26.85	82.8	31.93	12.10
$w^*_{\rm sfc}$ (m s^{-1})	0.7	0.07	0.62	0.14	6.69
ΔSWF (W m^{-2})	2.04	3.55	2.24	3.05	0.57
ΔLWF (W m^{-2})	−10.33	4.28	−6.63	3.84	8.67
ΔF_R (W m^{-2})	−8.49	1.99	−4.39	4.04	11.91
$w^*_{\rm rad}$ (m s^{-1})	0.51	0.15	0.34	0.17	10.01
w^* (m s^{-1})	0.80	0.08	0.68	0.13	10.35

which is located under the descending branch of the Hadley circulation. The ECMWF-model-reported temperature advection at 900 mb was negligible at both locations with the differences between them being statistically insignificant. The ECMWF-reported moisture advection at 900 mb was negligible over Manus and −1.43 g kg^{-1} day^{-1} over the Azores. These results from the ECMWF model collectively suggest that the cumuli over Manus formed locally with minimal influence of local gradients in temperature and moisture, while the cumuli over the Azores formed under dry advection conditions. The ECMWF-reported LHF was much higher than the SHF at both locations with the SHF higher over the Azores compared to that over Manus, with vice versa for the LHF.

The reported values of large-scale subsidence rates, tendency terms, and surface fluxes by the NCEP–NCAR reanalysis model differed significantly from those reported by the ECMWF reanalysis model (Table 3). As reported by the NCEP–NCAR reanalysis, the large-scale subsidence rate was negative over Manus and positive over the Azores, with both locations advecting cold and dry air at 900 mb during cumulus cloud conditions. The NCEP–NCAR model surface fluxes were lower than those reported by the ECMWF reanalysis model. It is beyond the scope of this study to explore the cause of the differences in the values reported by the two reanalysis models. For calculating the w^*, we have used the SHF and LHF values reported by the ECMWF reanalysis model. As the surface fluxes from the NCEP–NCAR reanalysis model are lower than those from the ECMWF reanalysis model, the subsequently calculated w^* from NCEP–NCAR will also be lower than that reported in Table 3, which is calculated from ECMWF-reported fluxes. The surface convective velocity scale ($w^*_{\rm sfc}$) calculated from the ECMWF model fluxes was slightly higher (0.7 m s^{-1}) over Manus than over the Azores (0.62 m s^{-1}).

The shortwave radiative flux divergence across the cloud layer is small (~2 W m^{-2}) at both locations. The longwave radiative flux divergence across the cloud layer was negative, suggesting boundary layer cooling at both locations with values of −10.33 W m^{-2} over Manus and −6.63 W m^{-2} over the Azores. The higher amount of longwave cooling over Manus is partly due to the greater cloud-layer thickness and partly due to higher values of temperature and moisture. The radiative velocity scale $w^*_{\rm rad}$ was lower than the surface convective velocity scale $w^*_{\rm sfc}$ at both locations, with values of 0.51 m s^{-1} over Manus and 0.34 m s^{-1} over the Azores. As the radiative velocity scale was ~70% of the value of the surface convective velocity scale over Manus and ~50% over the Azores, a significant role is played by the boundary layer cooling in maintaining turbulence within the boundary layer at these locations. The convective velocity scale w^* was higher over Manus (0.80 m s^{-1}) than over the Azores (0.68 m s^{-1}). The mean radar reflectivity within updrafts was higher

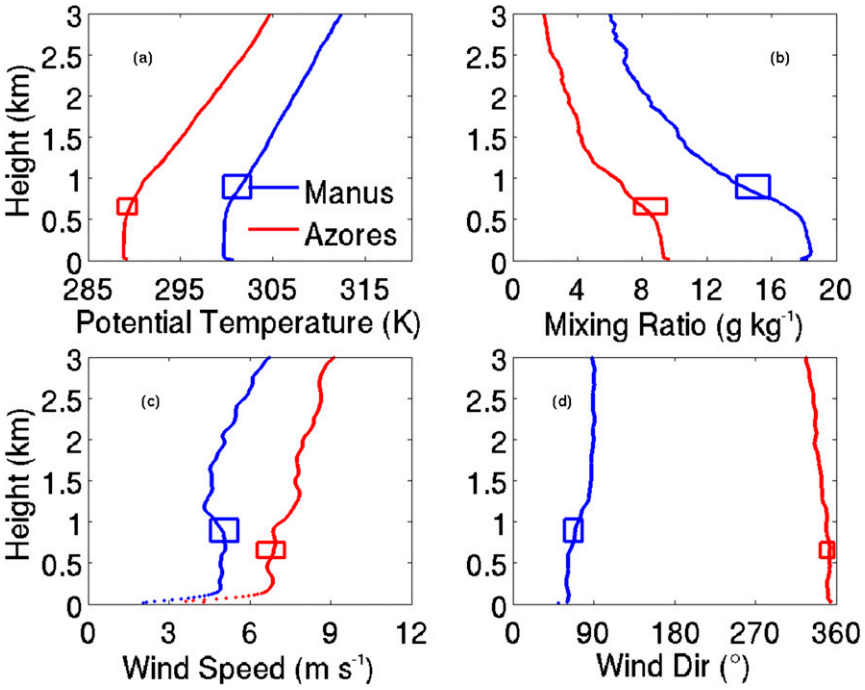

FIG. 3. Averaged profile of (a) potential temperature, (b) mixing ratio, (c) wind speed, and (d) wind direction, as a function of height for Manus and the Azores. The rectangles show the average locations of the cumulus cloud layers at the two sites.

over Manus as compared to the Azores and so was the mean updraft velocity. These analyses collectively suggest the cumulus-topped boundary layers over Manus are deeper, contain thicker clouds with larger cloud drops and have greater turbulence than those over the Azores. Despite higher mean in-cloud updraft velocities, because of the lower cloud cover, the updraft mass flux at $\eta = 0.2$ was lower over Manus as compared to that over the Azores. The distribution of updrafts and downdrafts within cumulus clouds did not exhibit statistically significant differences between the two locations, with 70% of the cloudy parcels being updrafts. However, the contribution of updrafts stronger than $1\,\mathrm{m\,s^{-1}}$ to the total cloud fraction near the cloud-layer base differed significantly between the two locations with the clouds over Manus containing much a higher percentage of updrafts stronger than $1\,\mathrm{m\,s^{-1}}$ (~22%) than those over the Azores (~12%). The same was true for downdrafts stronger than $-1\,\mathrm{m\,s^{-1}}$ at $\eta = 0.8$ with values of ~22% for Manus and ~12% for the Azores.

During the study period 43 radiosondes were launched at the Azores and 34 were launched at Manus. The averaged profiles of potential temperature, mixing ratio, wind speed, and wind direction at the two sites together with the cloud boundaries are shown in Fig. 3. A surface mixed layer can be seen at both of the locations in the profiles of potential temperature and mixing ratio, above which the cumulus clouds form. The mean potential temperature in the mixed layer (0–500 m) is ~288 K at the Azores and ~299 K at Manus, while the mean mixing ratio is $\sim 9\,\mathrm{g\,kg^{-1}}$ at the Azores and is $\sim 18\,\mathrm{g\,kg^{-1}}$ at Manus. The averaged profiles of potential temperature and mixing ratio do not show any inversion above the cloud layer, consistent with the previous observations that the inversion associated with the cumulus-topped boundary layers being weak and difficult to determine (Albrecht et al. 1979). The wind speed was relatively constant with height at both locations below 1 km except at the surface layer (below 100 m), indicating the minimal role of wind shear in generating turbulence in the observed cumulus-topped boundary layers. The wind direction was predominantly from the northeast over Manus and from the north over the Azores, consistent with the case selection criteria. The cloud boundaries of low-level clouds (<3 km) shown in Fig. 3 and those shown in Fig. 2 differ from each other, as Fig. 2 shows the cloud boundaries of the entire cloud population (nonprecipitating cumuli, precipitating cumuli, upper-level stratus, etc.) while Fig. 2 refers to boundary layer nonprecipitating cumulus.

The averaged profiles of equivalent potential temperature θ_e and saturation equivalent potential temperature θ_{es} along with the averaged cumulus cloud locations for

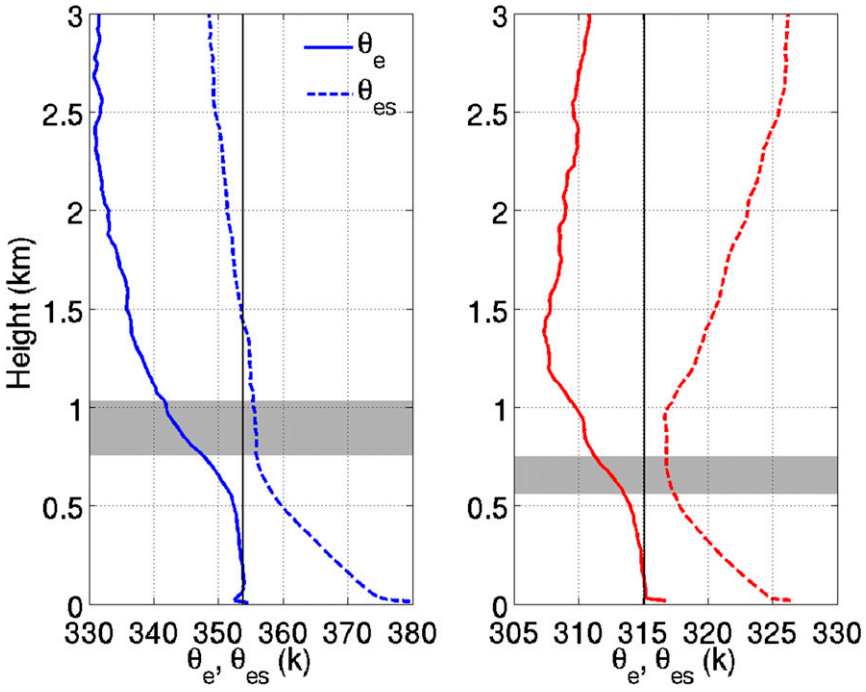

FIG. 4. Averaged profile of equivalent potential temperature θ_e and saturation equivalent potential temperature θ_{es} for the (left) Manus and (right) Azores cumulus cases. The vertical black line corresponds to the equivalent potential temperature at 100 m. The gray shading shows the averaged cloud location at each site.

Manus and the Azores are shown in Fig. 4. The equivalent potential temperature decreases by ~1 K from the surface to 500 m at both locations, indicating the mixed layer to be slightly dynamically unstable. For an undiluted air parcel rising from the surface there is no convective available potential energy (CAPE) present in the averaged sounding over the Azores, while substantial CAPE is present ~500 m above the cumulus cloud tops at Manus. Above the mixed layer, a clear trade wind inversion can be observed at the Azores, inhibiting the growth of the shallow cumuli, while the averaged profiles over Manus do not exhibit any inversion and had the level of free convection (LFC) at 1.5 km. Hence, in both locations, there is no environmental CAPE associated with boundary layer shallow cumuli as indicated by these averaged profiles.

The mean vertical profiles of hourly averaged shortwave, longwave, and net radiative fluxes along with the associated heating rate profiles are shown in Fig. 5. A downward flux is defined as positive, while an upward flux is defined as negative. The net longwave radiative flux decreases with height from the surface to the free troposphere at both locations, while the shortwave radiative flux increases with height from the surface to the free troposphere at both locations. Because of the higher water vapor loading in the tropical atmosphere, the downwelling longwave radiative flux (not shown) is higher at Manus, resulting in ~20 W m^{-2} lower values of the net longwave flux in the mixed layer over Manus as compared to the Azores. From 100 to 1100 m the longwave radiative flux decreased by ~30 W m^{-2} at the Azores while it decreased by ~37 W m^{-2} at Manus. Hence, the gradient of the decrease in longwave flux was higher at Manus than at the Azores. Because of the higher number of daytime observations at the Azores compared to Manus, the net shortwave flux in the mixed layer is ~100 W m^{-2} higher over the Azores than that over Manus.

The longwave radiative heating rate increased (less negative) from the surface to the cloud-layer base and decreased sharply near the cloud-layer top at both locations. The longwave radiative heating rate near the cloud-layer top was about -3 K day^{-1} at Manus and about -2.5 K day^{-1} at the Azores. Above the cloud-layer top, the longwave radiative cooling rate increased (less negative) with height at Manus, while it remained fairly constant at the Azores at around -2 K day^{-1}. The shortwave radiative heating rate increased sharply in the few hundred meters above the surface and remained fairly constant above that at both locations. The net radiative heating rate loosely follows the profile of the longwave radiative heating rate with reduced magnitude

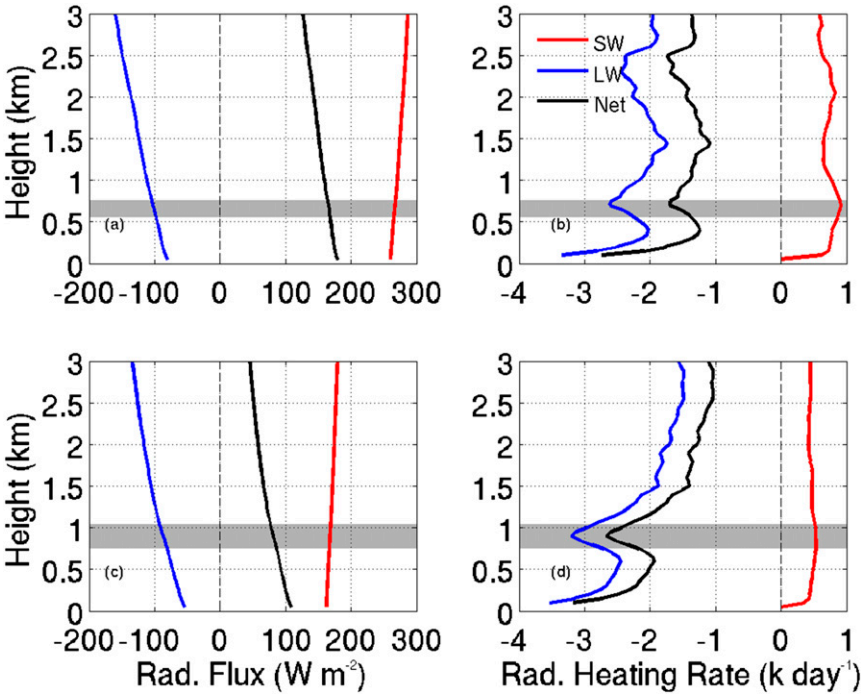

FIG. 5. (a),(b) Averaged profile of shortwave (SW), longwave (LW), and net radiative flux and associated heating rate for the Azores. (c),(d) As in (a),(b), but for Manus. The shading represents the average locations of cumulus clouds at the two sites.

at both locations. The profiles reported here are similar to those reported by Mather et al. (2007) for shallow clouds over Manus. The decrease in the longwave radiative heating rate near cloud-layer top is a clear indication of the impact of clouds on the boundary layer radiative cooling as compared to the clear-air boundary layer radiative cooling.

4. Cloud structure

The reflectivity reported by the vertically pointing Doppler cloud radar corresponds to the sixth moment of the drop size distribution (DSD). The histograms of radar reflectivity at four different cloud-layer depth-normalized levels (η) at the two locations are shown in Fig. 6. Also reported in each panel is the average reflectivity within updrafts (core) for each location. The range of the radar reflectivity increased with height in the cumuli over the Azores, while it remained relatively constant with height in cumuli over Manus. The change in the range of radar reflectivity with height at both locations is primarily due to shifting of the right edge of the spectrum to higher values. The radar reflectivity in core (updraft) samples in cumuli over the Azores increased with height by ~7 dBZ from η values of 0.2 to 0.8, while for the same change in height the reflectivity changed by 1.6 dBZ in cumuli over Manus. The mean radar reflectivity within core samples was higher in cumuli over Manus as compared to cumuli over the Azores at all levels. The difference in the radar reflectivity values at the two locations was greatest at $\eta = 0.2$. The higher value of radar reflectivity in cumulus clouds over Manus cannot be fully explained from these observations alone, while the potential reason for this might be in the different aerosol–cloud interactions between the tropics and the subtropics or simply because of the higher boundary layer RH. This collectively suggests that on average the cloud drops within cumuli over the Azores get bigger from cloud base to cloud top, while the same increase in diameter from cloud base to cloud top is relatively small for cumuli over Manus.

The histograms of in-cloud vertical velocity at four different cloud-layer depth-normalized levels at the two locations are shown in Fig. 7. Also reported in each panel is the mean updraft velocity at that level. The mean vertical velocity within the cloud layer decreased from cloud-layer base to the cloud-layer top at both locations. The mean vertical velocities at η levels 0.2, 0.4, 0.6, and 0.8 were 0.4, 0.31, 0.11, and 0.01 m s^{-1} over the Azores and 0.44, 0.26, 0.11, and -0.19 m s^{-1} over Manus. A decrease in the mean vertical velocity with height suggests an increased amount of downdrafts with

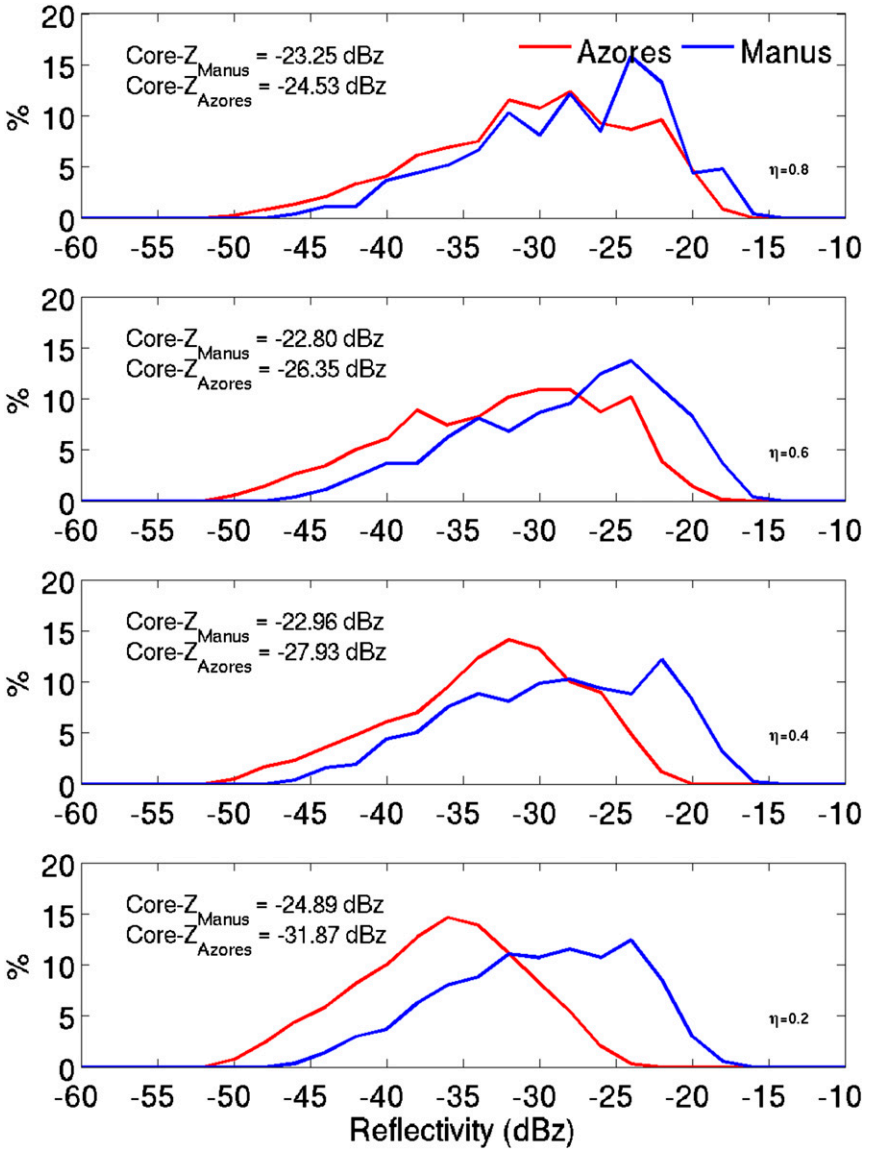

FIG. 6. Histogram of reflectivity at Manus (blue) and the Azores (red) at four different cloud-layer depth-normalized levels (0.2, 0.4. 0.6, and 0.8). The mean values of reflectivity within core (updrafts) samples at the two locations are also reported in each panel.

height and dilution of updrafts with height. The mean updraft (core) velocity increased from cloud-layer base to cloud-layer top over the Azores, while the same decreased over Manus. An increase in the updraft velocity with height is expected for undiluted air parcels that experience thermodynamic lift as they utilize CAPE as a result of being warmer and moister than the environment. A lack thereof for cumuli over Manus suggests the rising cloudy air parcels getting diluted, reducing their buoyancy as they rise. The standard deviations of the distribution were 0.64, 0.95, 1.13, and 1.26 m s^{-1} at η values of 0.2, 0.4, 0.6, and 0.8 over the Azores, while they were 0.91, 0.99, 0.99, and 1.06 m s^{-1} over Manus. This suggests that similar to the reflectivity, the variability in vertical velocity increased from cloud-layer base to top over the Azores, while over Manus it largely remained unchanged. The skewness of the distributions were 0.46, 0.64, −0.17, and 0.43 over the Azores at η values of 0.2, 0.4., 0.6, and 0.8. At the same levels the corresponding values over Manus were −0.45, −0.29, 0.10, and 0.14. Positive (negative) skewness of vertical velocity is indicative of narrower and stronger updrafts (downdrafts) compared to the broader and weaker downdrafts (updrafts). The vertical velocity skewness

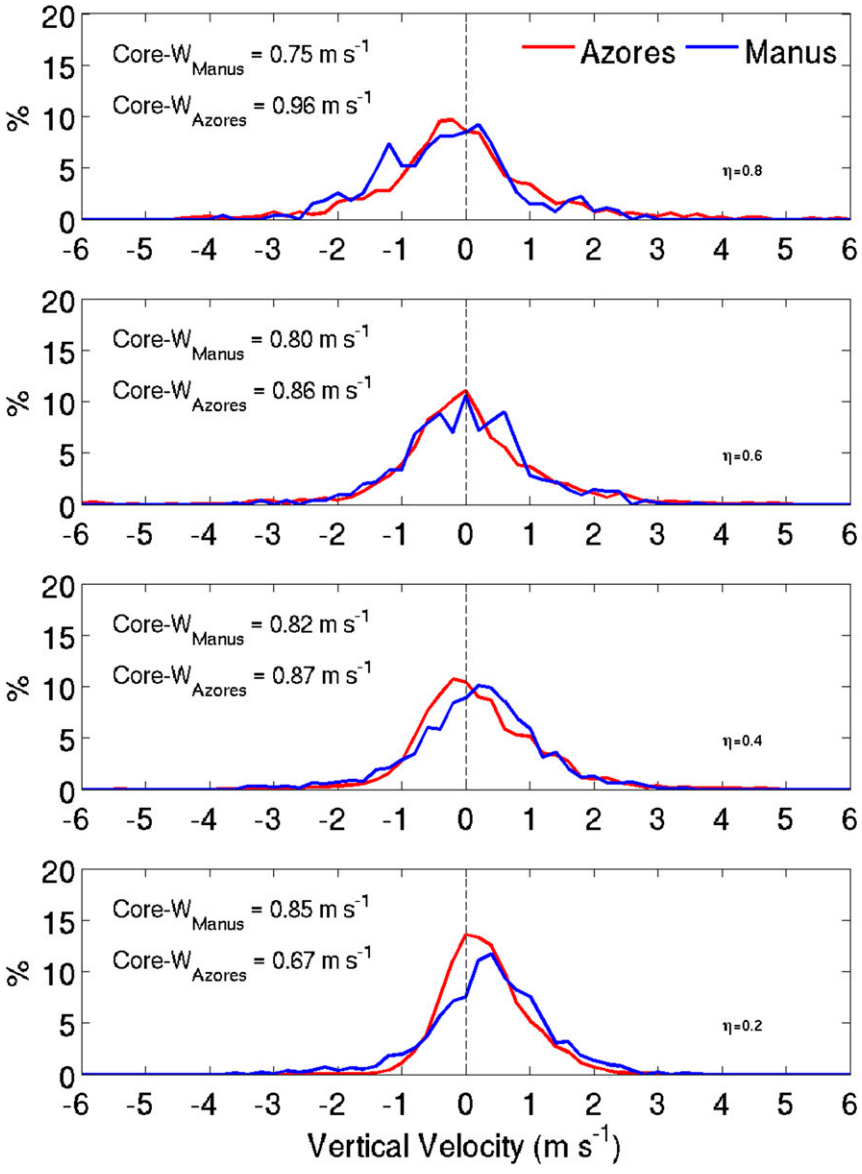

FIG. 7. Histogram of vertical velocity at Manus (blue) and the Azores (red) at four different cloud-layer depth-normalized levels (0.2, 0.4. 0.6, and 0.8). The mean values of vertical velocity within core (updrafts) samples at the two locations are also reported in each panel.

is positive in the entire cloud layer (except for $\eta = 0.6$) over the Azores, in agreement with previous observations of shallow cumulus clouds (Ghate et al. 2011; Rémillard et al. 2012). The vertical velocity skewness is negative in the lower half of the cloud layer and weakly positive in the upper half of the cloud layer over Manus. This along with higher values of radar reflectivity suggests the cumuli over Manus contain more downdrafts than updrafts along with bigger drops as compared to the cumuli over the Azores.

The mass flux as a function of vertical air motion at four cloud-layer depth-normalized levels for the two locations is shown in Fig. 8. Also reported in each panel is the mean updraft mass flux at each location. The mean updraft mass flux decreased with height at both locations. The updraft mass flux was greater than the downdraft mass flux at both locations at all heights, consistent with the conceptual model of cumulus clouds as bubbles of rising air from the mixed layer. The downdraft mass fluxes at η levels 0.2, 0.4, 0.6, and 0.8 over the Azores were -4.72, -7.03, -6.89, and $-4.24\,\mathrm{g\,m^{-2}\,s^{-1}}$, while those over Manus were -5.4, -5.52, -2.97, and $-2.37\,\mathrm{g\,m^{-2}\,s^{-1}}$. Hence, the ratio of the updraft mass flux to the downdraft mass flux

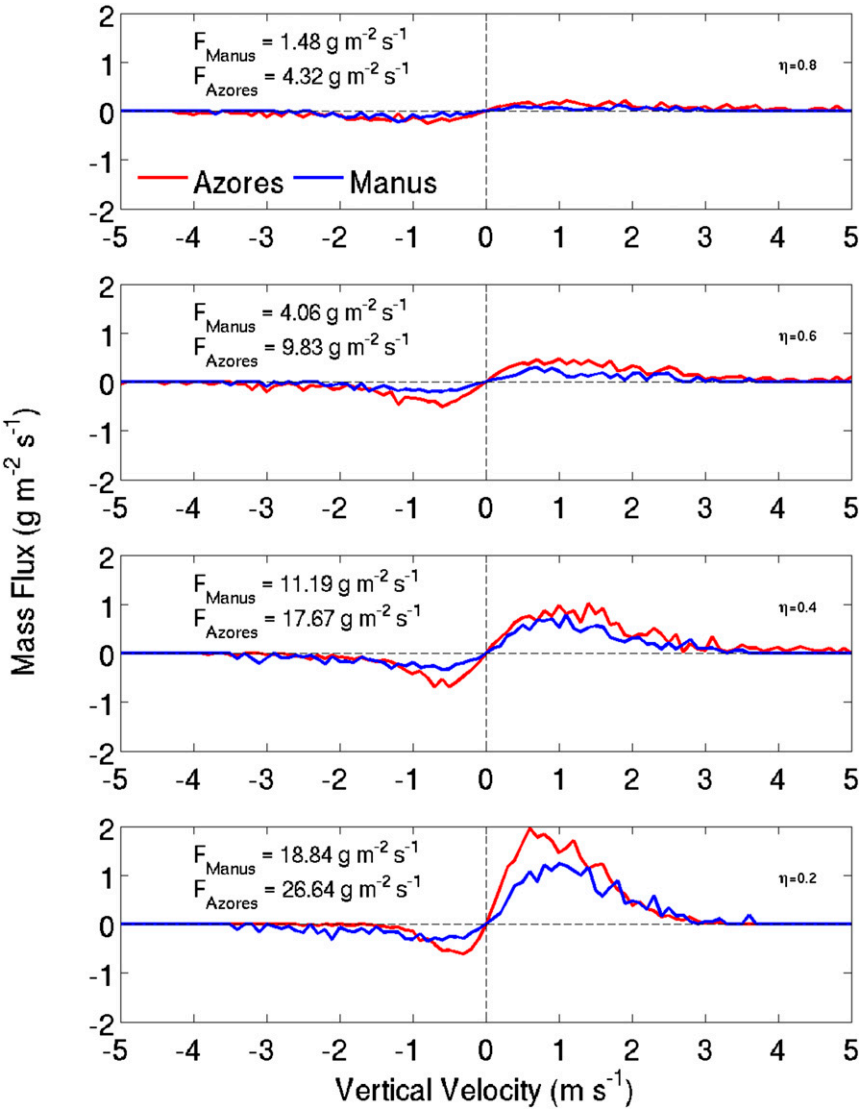

FIG. 8. Averaged velocity binned mass flux for the Azores and Manus at four different cloud-layer depth-normalized levels.

increased (in absolute value) with height at both locations. It is also noteworthy that at $\eta = 0.8$ on average the downdraft mass flux was almost twice that of the updraft mass flux. The mode of the distribution suggests that most of the mass is being transported by updrafts having velocities of $\sim 0.5\,\mathrm{m\,s^{-1}}$ over the Azores and $\sim 1\,\mathrm{m\,s^{-1}}$ over Manus at $\eta = 0.2$ with the mode of the distribution increasing with height at both locations. The amount of mass transported by updrafts with higher velocities ($>1\,\mathrm{m\,s^{-1}}$) increases with height at both locations, with the mass transported in cumuli over the Azores being much greater than the cumuli over Manus. This is partly due to higher vertical velocities observed in the cumuli over the Azores as compared to in the cumuli over Manus. Compared to the strong updrafts, a negligible amount of mass is being transported by downdrafts stronger than $-1\,\mathrm{m\,s^{-1}}$ at both locations.

Cloud-layer depth-normalized profiles of reflectivity and vertical velocity at both locations for all, core, and coherent samples are shown in Fig. 9, with one standard deviation of the profiles of core samples shown by the shading. The profiles of radar reflectivity differ between the locations, but do not exhibit any statistically significant changes between the three categories. This is consistent with past studies and suggests the sixth moment of the DSD to be similar regardless of the parcel buoyancy. The range (increase) of radar reflectivity from $\eta = 0$ to 0.8 is ~ 13 dBZ for cumuli over the Azores

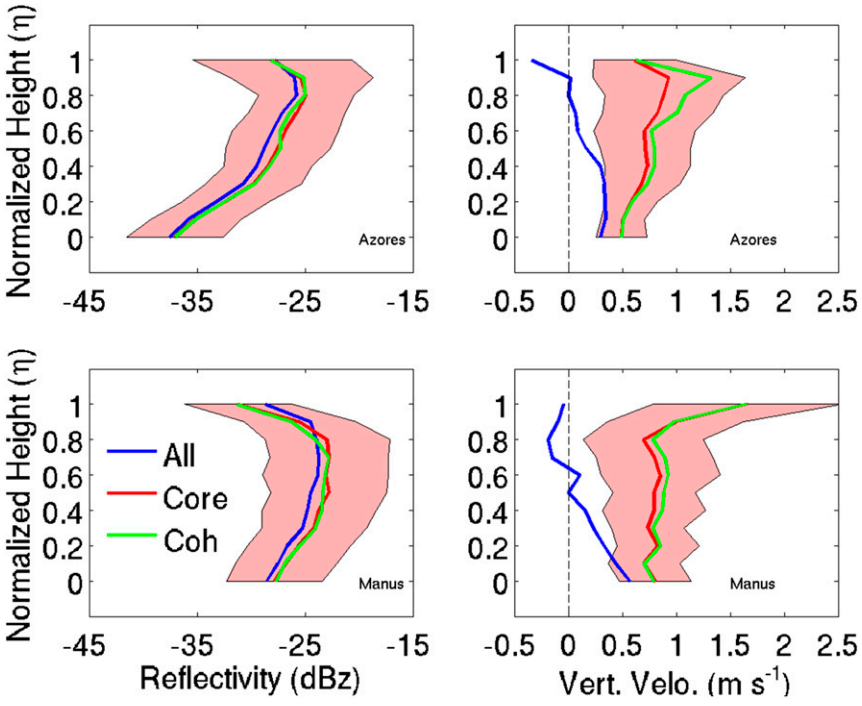

FIG. 9. Averaged cloud-layer depth-normalized profile of all, core, and coherent reflectivity and vertical velocity for (top) the Azores and for (bottom) Manus.

and is only ~5 dBZ for cumuli over Manus. As the radar reflectivity is heavily weighted by larger cloud drops, an increase in the radar reflectivity with height is indicative of an increase in the drop sizes, while the lack thereof suggests either a lack of an increase in drop size or the presence of other compensating mechanisms like a decrease in drop concentration. The profile of the radar reflectivity exhibited a decrease near the cloud-layer top (η = 0.8–1) at both locations, with the decrease being higher over Manus (~7 dBZ) than over the Azores (~2 dBZ).

The mean in-cloud vertical velocity decreased with height at both locations. It was positive in the lower half of the cloud layer and negative above over Manus, while it was positive below η = 0.8 over the Azores and negative above. The averaged updraft velocity within the cloud layer increased with height until η = 0.8 over the Azores with an increase of ~0.5 m s^{-1}, while it largely remained constant over Manus with a value of ~0.75 m s^{-1}. To be consistent with previous work, coherent updrafts were also identified that increased with height over the Azores and remained constant with height over Manus. Both the core and coherent updraft samples decreased in magnitude from η = 0.8 to 1 over the Azores, while they showed an increase over Manus at the same level. It is difficult to gauge the reason for this difference from these observations alone.

The profiles of averaged cloud fraction and mass flux at the two locations for all, core, and coherent samples are shown in Fig. 10. The peak of the cloud fraction is at η = 0.2 at both locations with values of ~2.75% over Manus and ~4.5% over the Azores. Over Manus and over the Azores, at η = 0.2 about 70% of the samples are core and about 54% are coherent. The contributions of coherent updrafts to the cloud fraction are similar over the two locations with values of ~54%, 40%, 30%, and 25% at η levels of 0.2, 0.4, 0.6, and 0.8, respectively. As a result of higher cloud coverage, the mass flux from all samples is higher at all levels over the Azores as compared to that over Manus. Because of the presence of more downdrafts, the mass flux is negative above η = 0.6 over Manus, while it is negative above η = 0.8 over the Azores. These results suggest that the updraft mass flux near cloud base over the Azores is about 35% higher compared to that over Manus during cumulus cloud conditions. The contributions of coherent updrafts to the updraft mass flux were similar at both location with values of 58%, 63%, 63%, and 70% at η levels of 0.2, 0.4, 0.6, and 0.8, respectively. Hence, although the contribution of coherent updrafts to the cloud fraction decreases with height, their contribution to the updraft mass flux increases with height at both locations.

The profiles of conditionally sampled mean updraft and downdraft fractions at the two locations as a

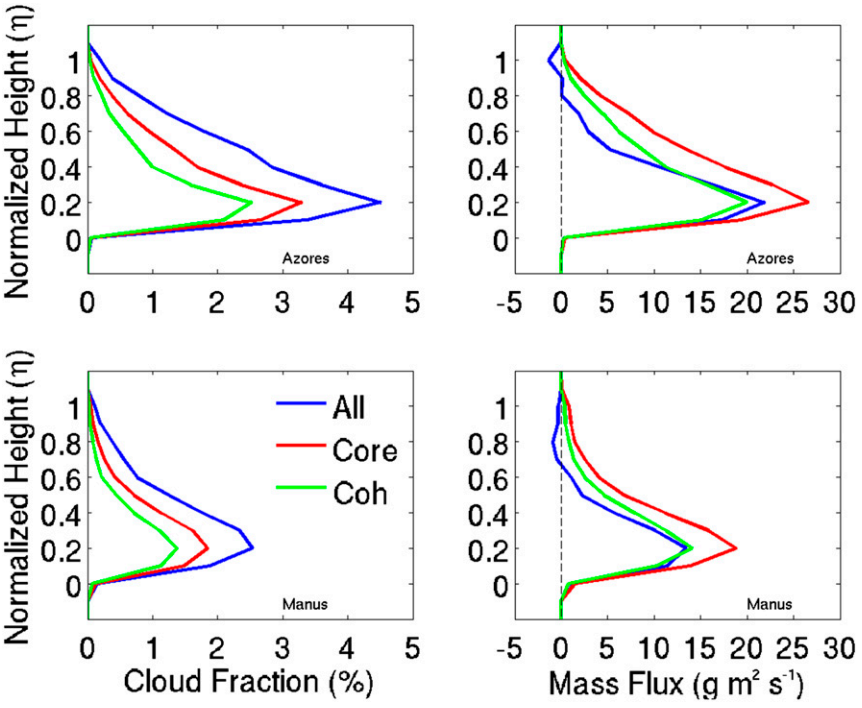

FIG. 10. Averaged cloud-layer depth-normalized profile of all, core, and coherent fraction and mass flux for (top) the Azores and for (bottom) Manus.

function of cloud layer normalized depth are shown in Fig. 11. The profiles of both the updraft and downdraft fraction peak at (or near) $\eta = 0.2$ at both locations. The amount of downdrafts stronger than $-1\,\mathrm{m\,s^{-1}}$ peaks near the middle of the cloud layer over the Azores, while the same peak is near $\eta = 0.2$ over Manus. Consistent with the theory of cumulus clouds being rising bubbles from the mixed layer, the clouds mainly consisted of updrafts (~70%) at both locations. Although the amount of updrafts near cloud base within the cloudy samples were similar at both locations (Table 2), the contribution of updrafts stronger than $1\,\mathrm{m\,s^{-1}}$ to the cloud fraction differed greatly between the locations. The contribution of updrafts stronger than $1\,\mathrm{m\,s^{-1}}$ to the cloud fraction decreased from ~22% at $\eta = 0.2$ to ~12% at $\eta = 0.8$ over Manus, while it remained relatively constant with height at ~13% over the Azores. The contribution of downdrafts to the cloud fraction decreased from ~22% near cloud-layer top to ~8% near cloud-layer base over Manus, while the decrease was from ~12% to 0.5% over the Azores. These results suggest that in addition to having vigorous circulations, the clouds over Manus contained a significant amount of saturated downdrafts in the entire cloud layer as compared to those over the Azores.

The seasonal changes in vertical velocity statistics were also explored. The seasonally averaged profiles of vertical velocity and radar reflectivity within core samples are shown in Fig. 12. The seasons were defined as winter [December–February (DJF)], spring [March–May (MAM)], summer [June–August (JJA)], and fall [September–November (SON)]. The number of samples differed between the seasons at the two locations (Table 1), making some of the differences statistically insignificant. The vertical velocity within updraft cores did not exhibit any statistically significant difference between the seasons at the two sites, with the seasonal differences at the Azores being more than those over Manus, while the radar reflectivity did exhibit pronounced differences between the seasons at both sites, with the differences being greater over the Azores. The radar reflectivity at the cloud base was highest during the winter months over the Azores and lowest during the summer months there, with the values being similar during the fall and spring seasons. Over the Azores the radar reflectivity increased from cloud base to cloud top during all seasons except spring (MAM), when it increased till the middle of the cloud and then remained almost constant till cloud top. Over Manus the radar reflectivity was lowest in the fall season, and similar in winter and spring seasons, with the values during summer in between the two. It is difficult to explain the changes in the radar reflectivity with seasons and lack of changes of vertical velocity at both sites. The changes in

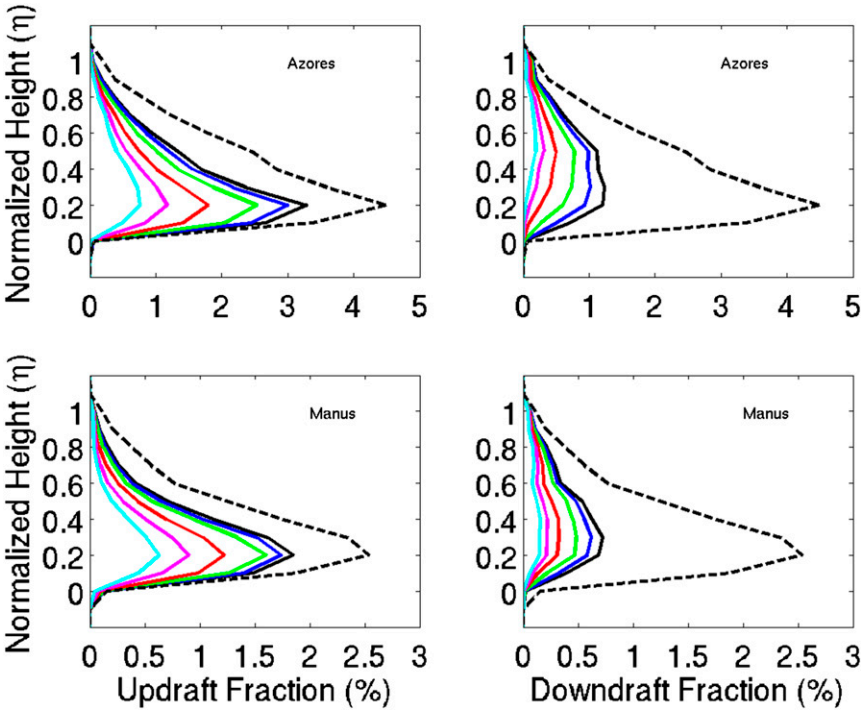

FIG. 11. Cloud-layer depth-normalized profiles of (left) mean hourly updraft fraction and (right) downdraft fraction for cumuli observed over (top) the Azores and (bottom) Manus. The values of conditionally sampled updrafts and downdrafts are similar in magnitude but opposite in sign. The lines correspond to the values of 0, black; 0.1, blue; 0.25, green; 0.5, red; 0.75, magenta; and 1 m s^{-1}, cyan. The profile of cloud fraction (dashed black line) is also shown in each panel for comparison purposes.

the radar reflectivity point toward changes in the background aerosol concentration, together with changes in environmental relative humidity.

5. Summary and discussion

In this study we have analyzed 166 h of data collected in the oceanic trade wind region and 197 h of data collected in the oceanic tropical region in cumulus cloud conditions to contrast the dynamical structure of the clouds observed in the two regions. As expected, the tropical cumulus-topped boundary layer had much lower large-scale subsidence at 700 mb (~4 mb day^{-1}) as compared to its subtropical counterpart (~87 mb day^{-1}). The lower subsidence rate resulted in a deeper boundary layer in the tropics as compared to the subtropics. Our data suggest the tropical shallow cumuli to be significantly thicker than the subtropical shallow cumuli, but with the cloud coverage higher in the subtropical boundary layer than at the tropical boundary layer. Although thicker, the averaged cloud chord length of tropical cumuli was significantly lower than that of the subtropical cumuli, which might be a consequence of a stronger inversion and higher BL wind speeds in the subtropics. The surface convective velocity scale and the radiative velocity scale were higher over the tropics than the subtropics, suggesting elevated levels of BL turbulence associated with tropical cumuli than the subtropical cumuli. The ratio of the radiative velocity scale to the surface convective velocity scale ranged from about 0.5 to 0.75 at the two locations, suggesting the importance of boundary layer radiation in generating turbulence together with the surface convection. Out of the 363 h of data analyzed in this study, the shortwave radiative heating off set the longwave cooling to inhibit turbulence generation during only 26 h, while the surface fluxes (SHF and LHF) were never negative at each location. This together with the lower standard deviation of w^*_{sfc} as compared to w^*_{rad}, suggests radiation to be the primary modulator of turbulence generation other than surface convection in the two cumulus-topped boundary layers. However, as the boundary layer cumulus clouds are inherently decoupled from the mixed layer, the turbulence generated by radiation might be limited only to the cloud layer.

The mean in-cloud radar reflectivity within updrafts and the mean updraft velocity were higher in tropical

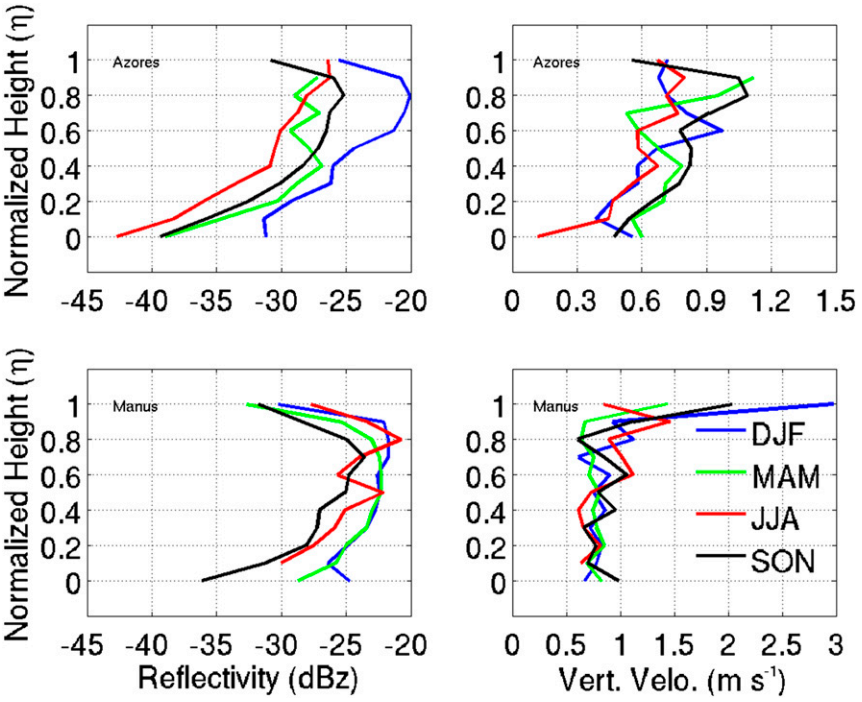

FIG. 12. Averaged cloud-layer depth-normalized profile of core reflectivity and vertical velocity for (top) the Azores and (bottom) Manus during four seasons.

cumuli than in the subtropical cumuli. Additionally, the radar reflectivity near cloud base in tropical clouds was ~10 dBZ higher than that during subtropical clouds. This suggests the cloud drops to be much bigger in tropical cumuli than in subtropical cumuli, making them more susceptible to precipitation. The values of radar reflectivity within all, core, and coherent samples were statistically similar to each other at both locations. Given that the radar reflectivity is heavily weighted toward larger cloud drops, this suggests the effect of entrainment to be primarily in evaporating smaller cloud drops. The mean in-cloud vertical velocity decreased with height at both locations with negative values being observed in the upper half of the cloud layer. The averaged in-cloud updraft velocity increased with height in cumuli over the Azores, but remained relatively constant in cumuli over Manus. Consistent with the concept of cumulus clouds being rising bubbles of air (Stull 1985), 70% of the cloudy samples were updrafts at both locations. The cumuli over Manus were composed of more updrafts (and downdrafts) stronger than 1 m s^{-1} (-1 m s^{-1}) than the cumuli over the Azores. Although the updrafts in cumuli over the Azores were weaker, because of the higher cloud cover, the mass flux was higher over the Azores than at Manus.

The in-cloud vertical air motion, core velocity, coherent velocity and mass flux as scaled by the convective velocity scale (w^*) for the two locations are shown in Fig. 13. The profiles of vertical velocity of the all, core, and coherent samples differ between the two locations because of the differences in the thermodynamic conditions and forcing. Although the unscaled shape of the profiles of the all, core, and coherent vertical velocities differ between the locations (Figs. 8 and 9), when scaled by w^* they exhibit similar values especially in the lower half of the cloud layer. Because the w^* calculated in this study does not take into account effects of buoyancy reversal, the differences near cloud top in the profiles shown in Fig. 11 are as expected. Although the shapes of the profiles of the updraft mass flux are similar at the two locations, scaling by w^* fails to converge the profiles. This suggests the vertical air motion (turbulence) is influenced more by the forcing (radiation and surface buoyancy) than the updraft mass flux.

Although many studies have reported surveys of shallow cumulus clouds observed over the tropics and the subtropics, to the authors' knowledge this is the first study that has compared the cumuli observed at both regions. The results reported in Tables 2 and 3 suggest that the tropical and subtropical cumuli have different properties, with most of the differences being statistically significant. The broader implication of this study will likely be realized in conjunction with high-resolution large eddy

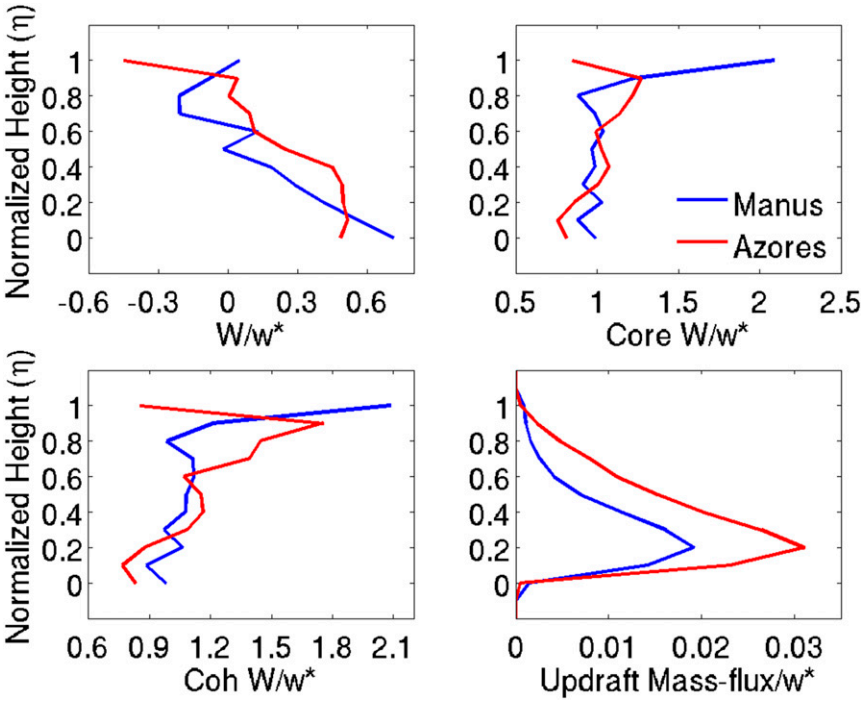

FIG. 13. Cloud-layer depth-normalized profiles of in-cloud vertical velocity, updraft (core) velocity, coherent updraft velocity, and mass flux as scaled by the convective velocity scale (w^*) at Manus (blue) and the Azores (red).

simulation (LES) model simulations of a few cases to verify and/or improve the cumulus parameterizations. Although the processes occurring in tropical and subtropical cumulus-topped marine boundary layers are similar, results presented here broadly suggest that the relative impact of those processes may differ significantly. This study also suggests that although the observations made by the vertically pointing Doppler cloud radar have been useful in characterizing their dynamic structure, collocated high-resolution observations of thermodynamic variables are needed to understand the thermodynamics–dynamics interactions that produce these clouds.

Acknowledgments. This work was primarily supported by the U.S. Department of Energy's (DOE) Atmospheric System Research (ASR), an Office of Science, Office of Biological and Environmental Research (BER) program, under Contract DE-AC02-06CH11357 awarded to Argonne National Laboratory. MAM was supported through ASR Grant DE-FG02-08ER64531 to Rutgers, The State University of New Jersey. Some of the data used in this study were obtained from the Atmospheric Radiation Measurement (ARM) Program sponsored by the U.S. Department of Energy, Office of Science, Office of Biological and Environmental Research, Climate and Environmental Sciences Division (CESD). The NCEP–NCAR reanalysis dataset was provided by the NOAA/OAR/ESRL PSD, Boulder, Colorado, from their website (http://www.esrl.noaa.gov/psd/).

REFERENCES

Albrecht, B. A., A. K. Betts, W. H. Schubert, and S. K. Cox, 1979: Model of the thermodynamic structure of trade wind boundary layer: Part I. Theoretical formulation and sensitivity studies. *J. Atmos. Sci.*, **36**, 73–89, doi:10.1175/1520-0469(1979)036<0073:MOTTSO>2.0.CO;2.

Arakawa, A., 2004: The cumulus parameterization problem: Past, present, and future. *J. Climate*, **17**, 2493–2525, doi:10.1175/1520-0442(2004)017<2493:RATCPP>2.0.CO;2.

Augstein, E., H. Riehl, F. Ostapoff, and V. Wagner, 1973: Mass and energy transports in an undisturbed Atlantic trade-wind flow. *Mon. Wea. Rev.*, **101**, 101–111, doi:10.1175/1520-0493(1973)101<0101:MAETIA>2.3.CO;2.

——, H. Schmidt, and F. Ostapoff, 1974: The vertical structure of the atmospheric planetary boundary layer in undisturbed trade winds over the Atlantic Ocean. *Bound.-Layer Meteor.*, **6**, 129–150, doi:10.1007/BF00232480.

Berg, L. K., W. I. Gustafson Jr., E. I. Kassianov, and L. Deng, 2013: Evaluation of a modified scheme for shallow convection: Implementation of CuP and case studies. *Mon. Wea. Rev.*, **141**, 134–147, doi:10.1175/MWR-D-12-00136.1.

Bolton, D., 1980: The computation of equivalent potential temperature. *Mon. Wea. Rev.*, **108**, 1046–1053, doi:10.1175/1520-0493(1980)108<1046:TCOEPT>2.0.CO;2.

Bretherton, C. S., and S. Park, 2008: A new bulk shallow-cumulus model and implications for penetrative entrainment feedback on updraft buoyancy. *J. Atmos. Sci.*, **65**, 2174–2193, doi:10.1175/2007JAS2242.1.

——, J. R. McCaa, and H. Grenier, 2004: A new parameterization for shallow cumulus convection and its application to marine subtropical cloud-topped boundary layers. Part I: Description and 1D results. *Mon. Wea. Rev.*, **132**, 864–882, doi:10.1175/1520-0493(2004)132<0864:ANPFSC>2.0.CO;2.

Chandra, A. S., P. Kollias, and B. A. Albrecht, 2013: Multiyear summertime observations of daytime fair-weather cumuli at the ARM Southern Great Plains Facility. *J. Climate*, **26**, 10 031–10 050, doi:10.1175/JCLI-D-12-00223.1.

Clothiaux, E. E., T. P. Ackerman, G. G. Mace, K. P. Moran, R. T. Marchand, M. A. Miller, and B. E. Martner, 2000: Objective determination of cloud heights and radar reflectivities using a combination of active remote sensors at the ARM CART sites. *J. Appl. Meteor.*, **39**, 645–665, doi:10.1175/1520-0450(2000)039<0645:ODOCHA>2.0.CO;2.

Comstock, J. M., A. Protat, S. A. McFarlane, J. Delanoë, and M. Deng, 2013: Assessment of uncertainty in cloud radiative effects and heating rates through retrieval algorithm differences: Analysis using 3 years of ARM data at Darwin, Australia. *J. Geophys. Res. Atmos.*, **118**, 4549–4571, doi:10.1002/jgrd.50404.

Davidson, B., 1968: The Barbados Oceanographic and Meteorological Experiment. *Bull. Amer. Meteor. Soc.*, **49**, 928–934.

Eastman, R., and S. G. Warren, 2013: A 39-yr survey of cloud changes from land stations worldwide 1971–2009: Long-term trends, relation to aerosols, and expansion of the tropical belt. *J. Climate*, **26**, 1286–1303, doi:10.1175/JCLI-D-12-00280.1.

——, and ——, 2014: Diurnal cycles of cumulus, cumulonimbus, stratus, stratocumulus, and fog from surface observations over land and ocean. *J. Climate*, **27**, 2386–2404, doi:10.1175/JCLI-D-13-00352.1.

ECMWF, 1994: The description of the ECMWF/WCRP level III-A global atmospheric data archive. ECMWF Rep. 00211, 48 pp. [Available online at http://cedadocs.badc.rl.ac.uk/1109/1/The_description_of_the_ECMWF-WCRP_Level_3-A_global_atmospheric_data_archive.pdf.]

Ghate, V. P., M. A. Miller, and L. DiPretore, 2011: Vertical velocity structure of marine boundary layer trade wind cumulus clouds. *J. Geophys. Res.*, **116**, D16206, doi:10.1029/2010JD015344.

——, ——, B. A. Albrecht, and C. W. Fairall, 2015: Thermodynamic and radiative structure of stratocumulus-topped boundary layers. *J. Atmos. Sci.*, **72**, 430–451, doi:10.1175/JAS-D-13-0313.1.

Golaz, J.-C., V. E. Larson, and W. R. Cotton, 2002: A PDF-based model for boundary layer clouds. Part I: Method and model description. *J. Atmos. Sci.*, **59**, 3540–3551, doi:10.1175/1520-0469(2002)059<3540:APBMFB>2.0.CO;2.

——, S. Wang, J. D. Doyle, and J. M. Schmidt, 2005: COAMPS-Les: Model evaluation and analysis of second-and third-moment vertical velocity budgets. *Bound.-Layer Meteor.*, **116**, 487–517, doi:10.1007/s10546-004-7300-5.

Iacono, M. J., E. J. Mlawer, S. A. Clough, and J.-J. Morcrette, 2000: Impact of an improved longwave radiation model, RRTM on the energy budget and thermodynamic properties of the NCAR Community Climate Model, CCM3. *J. Geophys. Res.*, **105**, 14 873–14 890, doi:10.1029/2000JD900091.

Ivanova, D. D., L. Mitchell, W. P. Arnott, and M. Poellot, 2001: A GCM parameterization for bimodal size spectra and ice mass removal rates in mid-latitude cirrus clouds. *Atmos. Res.*, **59–60**, 89–113, doi:10.1016/S0169-8095(01)00111-9.

Kalnay, E., and Coauthors, 1996: The NCEP/NCAR 40-Year Reanalysis Project. *Bull. Amer. Meteor. Soc.*, **77**, 437–470, doi:10.1175/1520-0477(1996)077<0437:TNYRP>2.0.CO;2.

Klein, S. A., Y. Zhang, M. D. Zelinka, R. Pincus, J. Boyle, and P. J. Gleckler, 2013: Are climate model simulations of clouds improving? An evaluation using the ISCCP simulator. *J. Geophys. Res. Atmos.*, **118**, 1329–1342, doi:10.1002/jgrd.50141.

Kollias, P., and B. Albrecht, 2010: Vertical velocity statistics in fair-weather cumuli at the ARM TWP Nauru Climate Research Facility. *J. Climate*, **23**, 6590–6604, doi:10.1175/2010JCLI3449.1.

——, M. A. Miller, E. P. Luke, K. L. Johnson, E. E. Clothiaux, K. P. Moran, K. B. Widener, and B. A. Albrecht, 2007: The Atmospheric Radiation Measurement program cloud profiling radars: Second-generation sampling strategies, processing, and cloud data products. *J. Atmos. Oceanic Technol.*, **24**, 1199–1214, doi:10.1175/JTECH2033.1.

——, ——, K. L. Johnson, M. P. Jensen, and D. T. Troyan, 2009: Cloud, thermodynamic, and precipitation observations in West Africa during 2006. *J. Geophys. Res.*, **114**, D00E08, doi:10.1029/2008JD010641.

Lappen, C.-L., D. Randall, and T. Yamaguchi, 2010: A higher-order closure model with an explicit PBL top. *J. Atmos. Sci.*, **67**, 834–850, doi:10.1175/2009JAS3205.1.

Larson, V. E., D. P. Schanen, M. Wang, M. Ovchinnikov, and S. Ghan, 2012: PDF parameterization of boundary layer clouds in models with horizontal grid spacings from 2 to 16 km. *Mon. Wea. Rev.*, **140**, 285–306, doi:10.1175/MWR-D-10-05059.1.

Li, Z., P. Zuidema, and P. Zhu, 2014: Simulated convective invigoration processes at trade wind cumulus cold pool boundaries. *J. Atmos. Sci.*, **71**, 2823–2841, doi:10.1175/JAS-D-13-0184.1.

Liu, C. L., and A. J. Illingworth, 2000: Toward more accurate retrievals of ice water content from radar measurements of clouds. *J. Appl. Meteor.*, **39**, 1130–1146, doi:10.1175/1520-0450(2000)039<1130:TMAROI>2.0.CO;2.

Lock, A. P., A. R. Brown, M. R. Bush, G. M. Martin, and R. N. B. Smith, 2000: A new boundary layer mixing scheme. Part I: Scheme description and single-column model tests. *Mon. Wea. Rev.*, **128**, 3187–3199, doi:10.1175/1520-0493(2000)128<3187:ANBLMS>2.0.CO;2.

Long, C. N., and Coauthors, 2013: ARM research in the equatorial western Pacific: A decade and counting. *Bull. Amer. Meteor. Soc.*, **94**, 695–708, doi:10.1175/BAMS-D-11-00137.1.

Mather, J. H., and J. W. Voyles, 2013: The ARM Climate Research Facility: A review of structure and capabilities. *Bull. Amer. Meteor. Soc.*, **94**, 377–392, doi:10.1175/BAMS-D-11-00218.1.

——, S. A. McFarlane, M. A. Miller, and K. L. Johnson, 2007: Cloud properties and associated radiative heating rates in the tropical western Pacific. *J. Geophys. Res.*, **112**, D05201, doi:10.1029/2006JD007555.

Matrosov, S. Y., T. Uttal, and D. A. Hazen, 2004: Evaluation of radar reflectivity–based estimates of water content in stratiform marine clouds. *J. Appl. Meteor.*, **43**, 405–419, doi:10.1175/1520-0450(2004)043<0405:EORREO>2.0.CO;2.

Miles, N. L., J. Verlinde, and E. E. Clothiaux, 2000: Cloud droplet size distributions in low-level stratiform clouds. *J. Atmos. Sci.*, **57**, 295–311, doi:10.1175/1520-0469(2000)057<0295:CDSDIL>2.0.CO;2.

Morcrette, J.-J., E. J. Mlawer, M. J. Iacono, and S. A. Clough, 2001: Impact of the radiation-transfer scheme RRTM in the ECMWF forecasting system, *ECMWF Newsletter*, No. 91, ECMWF, Reading, United Kingdom, 2–9. [Available online at http://www.ecmwf.int/sites/default/files/elibrary/2001/14633-newsletter-no91-summer-2001.pdf.]

Nam, C., S. Bony, J.-L. Dufresne, and H. Chepfer, 2012: The 'too few, too bright' tropical low-cloud problem in CMIP5 models. *Geophys. Res. Lett.*, **39**, L21801, doi:10.1029/2012GL053421.

Neggers, R., J. D. Neelin, and B. Stevens, 2007: Impact mechanisms of shallow cumulus convection on tropical climate dynamics. *J. Climate*, **20**, 2623–2642, doi:10.1175/JCLI4079.1.

Nuijens, L., and B. Stevens, 2012: The influence of wind speed on shallow marine cumulus convection. *J. Atmos. Sci.*, **69**, 168–184, doi:10.1175/JAS-D-11-02.1.

——, I. Serikov, L. Hirsch, K. Lonitz, and B. Stevens, 2014: The distribution and variability of low-level cloud in the North-Atlantic trades. *Quart. J. Roy. Meteor. Soc.*, **140**, 2364–2374, doi:10.1002/qj.2307.

Rauber, R. M., and Coauthors, 2007: Rain in shallow cumulus over the ocean: The RICO campaign. *Bull. Amer. Meteor. Soc.*, **88**, 1912–1928, doi:10.1175/BAMS-88-12-1912.

Rémillard, J., P. Kollias, E. Luke, and R. Wood, 2012: Marine boundary layer cloud observations in the Azores. *J. Climate*, **25**, 7381–7398, doi:10.1175/JCLI-D-11-00610.1.

Siebesma, A. P., and Coauthors, 2003: A large eddy simulation intercomparison study of shallow cumulus convection. *J. Atmos. Sci.*, **60**, 1201–1219, doi:10.1175/1520-0469(2003)60<1201:ALESIS>2.0.CO;2.

Stevens, B., and Coauthors, 2001: Simulations of trade wind cumuli under a strong inversion. *J. Atmos. Sci.*, **58**, 1870–1891, doi:10.1175/1520-0469(2001)058<1870:SOTWCU>2.0.CO;2.

Stull, R. B., 1985: A fair-weather cumulus cloud classification scheme for mixed-layer studies. *J. Climate Appl. Meteor.*, **24**, 49–56, doi:10.1175/1520-0450(1985)024<0049:AFWCCC>2.0.CO;2.

——, 1988: *An Introduction to Boundary Layer Meteorology*. Springer, 670 pp.

Troyan, D., 2012: Merged sounding value-added product. DOE/ARM Tech. Rep. DOE/SC-ARM/TR-087, 13 pp. [Available online at https://www.arm.gov/publications/tech_reports/doe-sc-arm-tr-087.pdf.]

vanZanten, M. C., and Coauthors, 2011: Controls on precipitation and cloudiness in simulations of trade-wind cumulus as observed during RICO. *J. Adv. Model. Earth Syst.*, **3**, M06001, doi:10.1029/2011MS000056.

Wang, Y., and B. Geerts, 2013: Composite vertical structure of vertical velocity in nonprecipitating cumulus clouds. *Mon. Wea. Rev.*, **141**, 1673–1692, doi:10.1175/MWR-D-12-00047.1.

Wood, R., and Coauthors, 2015: Clouds, aerosols, and precipitation in the marine boundary layer: An ARM Mobile Facility deployment. *Bull. Amer. Meteor. Soc.*, **96**, 419–440, doi:10.1175/BAMS-D-13-00180.1.

Zhang, Y., and S. A. Klein, 2013: Factors controlling the vertical extent of fair-weather shallow cumulus clouds over land: investigation of diurnal-cycle observations collected at the ARM Southern Great Plains site. *J. Atmos. Sci.*, **70**, 1297–1315, doi:10.1175/JAS-D-12-0131.1.